IJFAC

Indonesian Journal of Fundamental and Applied Chemistry

Article http://ijfac.unsri.ac.id

Synthesis, Characterization and Antibacterial Activity of Rice Husk Biochar/$MnFe_2O_4$ Nanocomposites

Oka Yana Afrizki[1], Poedji Loekitowati Hariani[1]*, Nabila Aprianti[2]

[1] Master's Program in Chemistry, Faculty of Mathematics and Natural Science, Sriwijaya University, Jln. Raya Palembang Prabumulih KM 32 Indralaya Ogan Ilir, Indonesia, 30662

[2] Research Center for Energy Conversion and Conservation, National Research and Innovation Agency (BRIN), B.J. Habibie Science and Technology Park, South Tangerang, Indonesia, 15313

*Corresponding Author: hariani.puji@gmail.com

Abstract

The increasing contamination with microorganisms has driven the development of effective, environmentally friendly antibacterial materials. Biochar was used as a porous matrix to support the dispersion of $MnFe_2O_4$ particles and to enhance the material's surface area. This study aims to synthesize a rice husk–based biochar/$MnFe_2O_4$ composite and evaluate its structural and morphological characteristics, as well as antibacterial activity. The composite was synthesized by coprecipitation and characterized by X-ray Diffraction (XRD), Scanning Electron Microscopy–Energy Dispersive X-ray Spectroscopy (SEM–EDX), and Fourier Transform Infrared Spectroscopy (FTIR). Antibacterial activity was evaluated using the disk diffusion method against Escherichia coli (Gram-negative) and Staphylococcus aureus (Gram-positive) at concentration variations of 1000–5000 mg/L. XRD results confirmed the formation of a spinel $MnFe_2O_4$ phase, as indicated high-intensity diffraction peaks at 31.56° and 35.22° and the average crystallite size calculated using the Scherrer equation was approximately 27.1 nm, indicating the formation of nanocrystalline domains. SEM analysis revealed that $MnFe_2O_4$ nanoparticles were uniformly dispersed on the biochar surface, while EDX confirmed the presence of C, O, Mn, and Fe elements. FTIR analysis identified –OH, C=O, and C–O functional groups, along with characteristic Mn–O and Fe–O vibrations, confirming successful composite formation. Antibacterial activity increased with concentration, reaching a maximum inhibition zone of 7.2 mm against both E. coli and S. aureus at 5000 mg/L, indicating mild antibacterial performance. The composite exhibits eco-friendly characteristics due to its biomass-derived biochar matrix and offers magnetic separability, facilitating easy recovery and potential reuse for sustainable environmental applications.

Keywords: Rice husk biochar, $MnFe_2O_4$, antibacterial activity

Article Info

Received 16 January 2026
Received in revised 24 February 2026
Accepted 25 February 2026
Available Online 28 February 2026

Abstrak (Indonesian)

Peningkatan kontaminasi oleh mikroorganisme telah mendorong pengembangan material antibakteri yang efektif dan ramah lingkungan. Biochar digunakan sebagai matriks berpori untuk mendukung dispersi partikel $MnFe_2O_4$ serta meningkatkan luas permukaan material. Penelitian ini bertujuan untuk mensintesis komposit biochar/$MnFe_2O_4$ berbasis sekam padi dan mengevaluasi karakteristik struktur, morfologi, serta aktivitas antibakterinya. Komposit disintesis menggunakan metode kopresipitasi dan dikarakterisasi dengan X-ray Diffraction (XRD), Scanning Electron Microscopy–Energy Dispersive X-ray (SEM–EDX), dan Fourier Transform Infrared Spectroscopy (FTIR). Aktivitas antibakteri diuji menggunakan metode difusi cakram terhadap *Escherichia coli* (Gram-negatif) dan *Staphylococcus aureus* (Gram-positif) pada variasi konsentrasi

1000–5000 mg/L. Hasil XRD mengonfirmasi pembentukan fase spinel $MnFe_2O_4$ yang ditunjukkan oleh puncak difraksi intensitas tinggi pada 31,56° dan 35,22, dengan ukuran kristalit rata-rata yang dihitung menggunakan persamaan Scherrer sebesar 27,1 nm, yang menunjukkan terbentuknya domain nanokristalin. Analisis SEM menunjukkan partikel $MnFe_2O_4$ terdispersi merata pada permukaan biochar, sementara EDX mengonfirmasi keberadaan unsur C, O, Mn, dan Fe. Analisis FTIR mengidentifikasi gugus –OH, C=O, dan C–O serta pita khas Mn–O dan Fe–O yang mengonfirmasi keberhasilan pembentukan komposit. Aktivitas antibakteri meningkat seiring dengan peningkatan konsentrasi, dengan zona hambat maksimum sebesar 7,2 mm terhadap *E. coli* dan *S. aureus* pada konsentrasi 5000 mg/L, yang menunjukkan kinerja antibakteri tergolong ringan. Komposit ini memiliki karakteristik ramah lingkungan karena berbasis biomassa sekam padi serta memiliki sifat kemagnetan yang memungkinkan pemisahan dan pemulihan yang mudah untuk potensi aplikasi lingkungan yang berkelanjutan.

Kata Kunci: Biochar sekam padi, $MnFe_2O_4$, aktivitas antibakteri

INTRODUCTION

Recent developments in materials science have focused on environmentally friendly multifunctional antibacterial materials [1]. Pathogenic microorganisms such as *Escherichia coli* (Gram-negative) and *Staphylococcus aureus* (Gram-positive) are common environmental contaminants. These bacteria were selected as representative models of Gram-negative and Gram-positive pathogens to evaluate the broad-spectrum antibacterial potential of the developed composite [2]. Biomass-derived biochar and magnetic manganese ferrite ($MnFe_2O_4$) have attracted attention due to their physicochemical stability and biological activity [3].

Biochar is a carbon-rich porous material produced through biomass pyrolysis, characterized by abundant surface functional groups that enable interactions with pollutants and microorganisms [4,5]. Rice husk, an abundant agricultural waste rich in carbon and silica, represents a sustainable and low-cost precursor for biochar production [5]. However, pristine biochar exhibits limited antibacterial activity, necessitating surface modification to enhance its functionality [5].

The functional properties of biochar were enhanced through modification with magnetic $MnFe_2O_4$ [6]. $MnFe_2O_4$ is a magnetic spinel ferrite known for its chemical stability, strong magnetic properties, and ability to generate reactive oxygen species (ROS) that can damage bacterial cell walls [6,7]. Surface Fe and Mn ions may also interfere with bacterial metabolic processes and membrane permeability, contributing to antibacterial effects [7,8]. Incorporating $MnFe_2O_4$ into biochar enhances antibacterial performance while enabling magnetic separation and reusability [9,10,11].

In this study, a rice husk–derived biochar/$MnFe_2O_4$ composite was synthesized via a coprecipitation method to develop a sustainable magnetic antibacterial material [6,9]. The novelty of this work lies in the utilization of agricultural waste (rice husk) as a biochar precursor combined with magnetic $MnFe_2O_4$ to produce an eco-friendly composite with dual functionality, antibacterial activity and magnetic separability [10-12]. The composite was characterized using XRD, SEM–EDX, and FTIR to evaluate its structural and surface properties prior to antibacterial testing against *E. coli* and *S. aureus* [7,13]. This approach provides a low-cost and environmentally sustainable strategy for developing biomass-based magnetic antibacterial materials for sustainable environmental applications [14,15].

MATERIALS AND METHODS

Materials

The materials used include biochar from rice husk is taken from the village of Pulau Harapan Banyuasin, manganese (II) chloride tetrahydrate ($MnCl_2{\cdot}4H_2O$) from Merck PA, iron (III) chloride hexahydrate ($FeCl_3{\cdot}6H_2O$) from Merck PA, dimethyl Sulfoxide (DMSO) from Merck PA, filter paper, disc paper, sodium hydroxide (NaOH) from Merck PA, amoxicillin from Merck PA, nutrient agar from Merck PA, deionized water.

Methods

Synthesis of Rice Husk Biochar

The synthesis of Biochar/$MnFe_2O_4$ was based on the co-precipitation method. A total of 2 g of biochar, 1.188 g of $MnCl_2.4H_2O$ and 3.240 g of $FeCl_3.6H_2O$ (molar ratio of Mn: Fe = 1:2) were dissolved in 150 mL of distilled water and stirred using an ultrasonic bath for 30 minutes. The pH was adjusted to 10-11 with NaOH 1 M under stirring, added dropwise, and the mixture was heated on a hotplate at 70 °C for 1 hour. The suspension was left at room temperature for 3 hours. The solid was centrifuged for 10 minutes, the residue was washed with distilled water, then dried and pyrolyzed at 550 °C for 1 hour with a heating rate of 10 °C min–1 to obtain Biochar/$MnFe_2O_4$ [17].

Characterization Nanocomposites

Biochar/$MnFe_2O_4$ nanocomposites were characterized using the XRD SmartLab Rigaku: Cu-Kα (λ = 1,5406 Å), 2θ range (10–90°), step size (0,02°). Biochar/$MnFe_2O_4$ nanocomposites were synthesized and analyzed using FTIR spectroscopy: wavenumber range (400–4000 cm^{-1}), resolution (4 cm^{-1}). The morphology and elemental composition of the Biochar/$MnFe_2O_4$ nanocomposites were determined using a Scanning Electron Microscopy–Energy Dispersive X-ray (SEM–EDX) JOEL JSM-IT200: accelerating voltage (15.00 kV).

Antibacterial Activity Test

Antibacterial activity was evaluated using the Kirby–Bauer disc diffusion method against *Escherichia coli* ATCC 25922 and *Staphylococcus aureus* ATCC 25923. The bacterial strains were cultured on Mueller–Hinton Agar (MHA) and incubated at 37°C for 24 h. The bacterial suspension was adjusted to 0.5 McFarland standard (10^8 CFU/mL) before testing. The nanocomposite was dispersed in DMSO solvent then vortexed for 5 minutes to obtain a homogeneous suspension. Each paper disc was dripped with 20 µL of nanocomposite solution with a concentration variation of 1000–5000 mg/L. Amoxicillin was used as a positive control, while DMSO served as a negative control. The disc containing the solution was placed on a solid medium that had been inoculated with the test bacteria, then incubated at 37 °C for 24 hours. After incubation, antibacterial activity was observed based on the formation of a clear zone around the disc (inhibition zone). The test was carried out three times.

Inhibition zone = inhibition zone diameter – well diameter

RESULT AND DISCUSSION

Biochar was successfully synthesized from rice husk through a pyrolysis process at a temperature of 450 °C for 1 hour under limited oxygen conditions. This process induced the decomposition of the main components of rice husk, such as cellulose, hemicellulose, and lignin, into solid carbon known as biochar [4,18]. The carbonization process promoted the removal of volatile compounds and enhanced the formation of an amorphous carbon structure, as typically indicated by the development of a porous texture and increased fixed carbon content [18,19]. The resulting porous structure contributes to a higher surface area, which is advantageous for its application as a supporting matrix in metal oxide composite synthesis [18].

The synthesis of the biochar/$MnFe_2O_4$ composite was carried out using the coprecipitation method, which is one of the most effective approaches for producing ferrites with fine particle sizes and homogeneous distribution [11,20]. In this process, precursor solutions of $FeCl_3 \cdot 6H_2O$ and $MnCl_2 \cdot 4H_2O$ were mixed in a stoichiometric ratio, followed by the addition of NaOH solution until the pH reached approximately 10 to form a metal oxide precipitate [11,20]. The introduction of biochar during the precipitation process enabled $MnFe_2O_4$ particles to adhere to and disperse uniformly on the biochar surface through electrostatic interactions and chemical bonding between carbon functional groups and metal ions [9,11,20].

The synthesized composite exhibited magnetic responsiveness, which qualitatively confirmed the formation of the $MnFe_2O_4$ ferrite phase. The incorporation of metal oxide particles into the biochar matrix is expected to modify the surface characteristics and enhance its functional properties, particularly for antibacterial and environmental applications [9,11].

Characterization Results

Characterization using XRD was aimed at obtaining the 2θ angle position, peak intensity, and crystal phase and determining the success of the nanocomposite synthesis. **Figure 3** displays the diffractogram of the Biochar/$MnFe_2O_4$ nanocomposite.

X-ray Diffraction (XRD) characterization was conducted to identify the crystalline phases, 2θ angular positions, and peak intensities, as well as to confirm the successful synthesis of the biochar/$MnFe_2O_4$ composite [10]. The resulting diffractogram is presented in **Figure 3.** XRD analysis is a widely used technique for confirming the formation of crystalline structures in metal oxide materials and biochar-based composites [3].

The main diffraction peaks were detected at 2θ positions of 24.98°, 31.56°, 35.22°, 43.39°, 50.97°, and 62.73°. These diffraction patterns show a strong correlation with the standard JCPDS data for $MnFe_2O_4$ (No. 74-2403), which exhibits characteristic peaks corresponding to the (220), (311), (400), (422), (511), and (440) crystal planes, thereby confirming the successful formation of the $MnFe_2O_4$ spinel phase within the composite [21,22,23]. The high-intensity peaks observed at 31.56° and 35.22° are typical features of the spinel structure, particularly the (311) plane, which is recognized as the dominant peak of $MnFe_2O_4$ These results confirm the successful

crystallization of the ferrite phase within the composite [23,24].

The crystallite size of $MnFe_2O_4$ was calculated using the Scherrer equation. The calculated crystallite size ranged from 5.7 to 80.3 nm depending on the selected reflection, with an average value of approximately 27,1 nm. The variation in crystallite size among different peaks may be attributed to differences in peak broadening, lattice strain, and instrumental effects [25]. The average nanoscale crystallite size confirms that the coprecipitation method successfully produced nanocrystalline $MnFe_2O_4$ domains dispersed within the biochar matrix [25].

The biochar used as the matrix is generally amorphous in nature and therefore does not produce sharp diffraction peaks. In addition to the sharp ferrite peaks, a broad diffraction feature centered around 2θ ≈ 24.98° was observed, which corresponds to the amorphous carbon structure of rice husk-derived biochar. This broad hump in the 20–30° region is characteristic of disordered carbon materials and reflects the arrangement of aromatic carbon layers [25,26]. The persistence of this amorphous background in the composite diffractogram indicates that the biochar framework remains structurally intact after $MnFe_2O_4$ incorporation. Rather than interfering with ferrite crystallization, the amorphous biochar matrix likely provides a porous support that dispersion of $MnFe_2O_4$ nanoparticles. This structural combination of crystalline ferrite domains embedded in an amorphous carbon matrix is advantageous for multifunctional performance, as the biochar enhances surface area and adsorption capability while $MnFe_2O_4$ contributes magnetic [25,26].

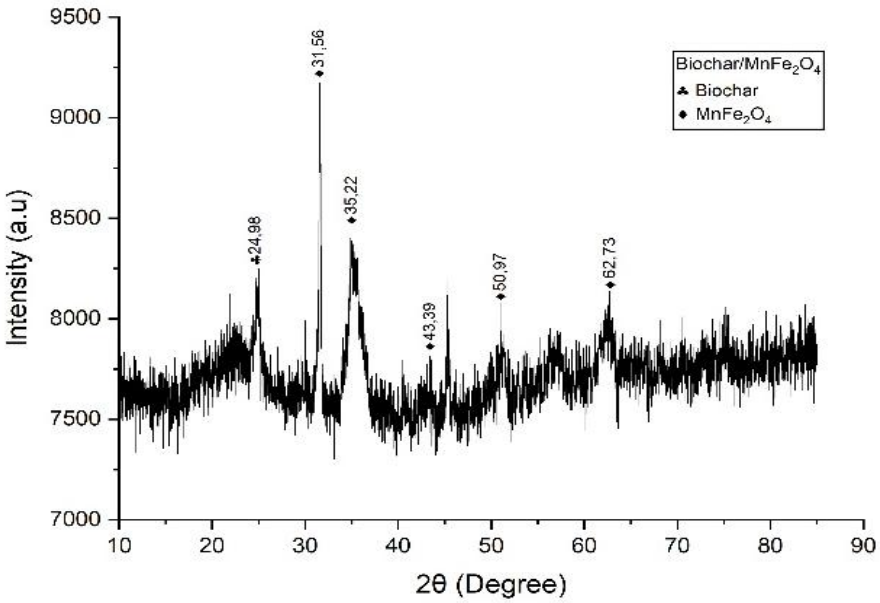

Figure 3. XRD pattern of the biochar/$MnFe_2O_4$ nanocomposite, showing characteristic peaks of the cubic spinel phase (JCPDS No. 74-2403).

SEM characterization was performed to observe the morphology of Biochar/$MnFe_2O_4$ nanocomposite. The results of the nanocomposite characterization using SEM are shown in **Figure 4.** The surface morphology of rice husk biochar observed by Scanning Electron Microscopy (SEM) in **Figure 4 (a)** shows that the biochar possesses a porous structure with irregular shapes, which is a common characteristic of biochar produced through biomass pyrolysis [9,10]. Based on the 10 µm scale bar, the pore diameters are estimated to range from approximately 2 to 8 µm. The formation of these macropores is attributed to the release of volatile components during thermal decomposition, resulting in an increased surface area and rough surface texture. [9,10]. After the incorporation of $MnFe_2O_4$, the biochar surface appears to be covered by fine granular particles distributed across the surface. Although slight localized agglomeration can be observed in certain regions, no severe bulk clustering is evident at this magnification, indicating relatively good dispersion of $MnFe_2O_4$ within the biochar matrix [9,10].

The uniform distribution of magnetic particles increases the contact area between the biochar and the surrounding environment, thereby enhancing the

effectiveness of interactions with bacteria. The rough and porous surface also plays an important role in enlarging the adsorption area, allowing intensive interactions between the material and microorganisms, which can ultimately disrupt cellular metabolism and lead to bacterial inactivation [9,27,28].

Energy Dispersive X-ray (EDX) analysis in **Figure 4 (b)** confirmed the presence of the main constituent elements, namely C, O, Mn, and Fe, with carbon as the dominant component originating from biochar and Mn and Fe proportions indicating the formation of $MnFe_2O_4$ [9,10].

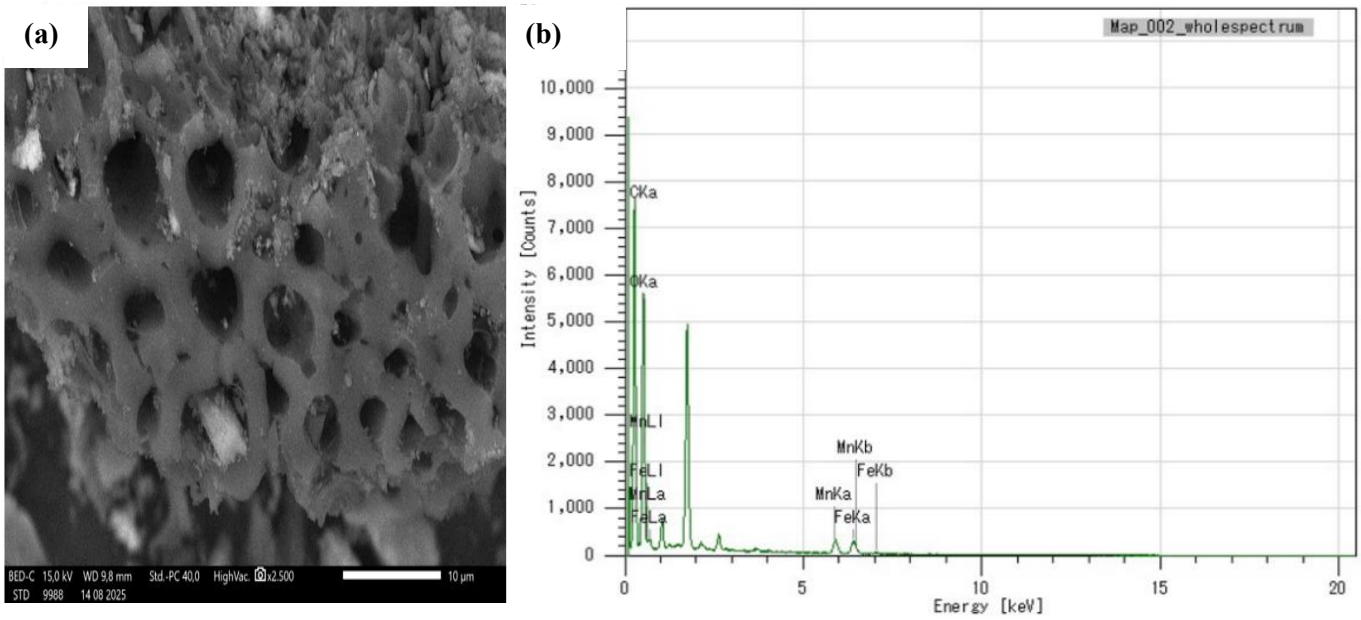

Figure 4. SEM-EDX micrograph of the biochar/$MnFe_2O_4$ composite showing porous biochar structure with uniformly dispersed $MnFe_2O_4$ nanoparticles on the surface.

Table 1. Semi-quantitative elemental composition of biochar/$MnFe_2O_4$ composite obtained from EDX analysis.

Element	Mass (%)	Atomic (%)
C	47.05	58.27
O	41.59	38.67
Mn	5.58	1.51
Fe	5.79	1.54

Energy Dispersive X-ray (EDX) analysis **Figure 4 (b)** confirmed the presence of C, O, Mn, and Fe as the main constituent elements of the biochar/$MnFe_2O_4$ composite **Table 1**. Carbon was the dominant element with a mass 47.05% and atomic 58.27%, originating from the biochar matrix, while oxygen with a mass 41.59% and atomic 38.67% is associated with surface functional groups and metal–oxygen bonds in $MnFe_2O_4$. The presence of Mn with a mass 5.58% and atomic 1.51%, and Fe with a mass 5.79% and atomic 1.54% verifies the successful incorporation of manganese ferrite. The absence of other elements in significant amounts suggests that the washing and purification processes were carried out effectively. These EDX results further support that the synthesized composite material consists of biochar as the carbon matrix and $MnFe_2O_4$ as the active magnetic phase [9,10].

Characterization using FTIR to determine the functional groups in Biochar/$MnFe_2O_4$ nanocomposite synthesis **Figure 5**. displays the spectrum of the Biochar/$MnFe_2O_4$ nanocomposite.

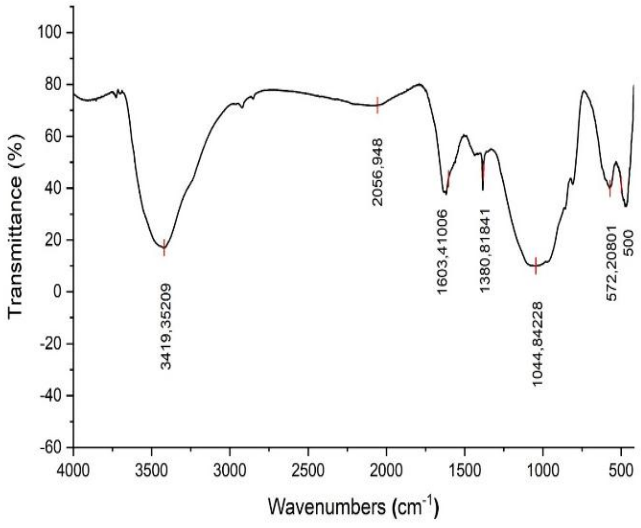

Figure 5. FTIR spectrum of the biochar/$MnFe_2O_4$ composite

Fourier Transform Infrared (FTIR) analysis was conducted to identify the functional groups present in the Biochar/$MnFe_2O_4$ composite and to confirm the successful interaction between biochar and the metal oxide components [30]. The FTIR spectrum of the composite is presented in **Figure 5**. FTIR analysis is a widely used technique for investigating the presence of surface functional groups and chemical interactions in biochar-based materials and metal oxide composites [9,29,30].

The FTIR spectrum exhibits a relatively broad absorption band at 3419,35 cm^{-1}, which is characteristic of O–H stretching vibrations from hydroxyl groups [30]. These groups may originate from residual organic compounds in the biochar or from water molecules adsorbed on the material surface, and are commonly observed in carbon-based materials [31]. The presence of O–H functional groups contributes to the enhanced hydrophilicity of the composite surface and facilitates interactions between the material and its surrounding environment [30,31].

The weak absorption band observed at 2056,94 cm^{-1} is not typically characteristic of pristine biochar. This region is generally associated with combination bands, overtone vibrations, or possible interactions involving surface functional groups and metal species. Therefore, this band may be attributed to secondary vibrational effects rather than a primary functional group [33]. Furthermore, the band observed at 1603,41 cm^{-1} is attributed to aromatic C=C vibrations of the graphitic framework of biochar, indicating that the aromatic carbon structure remains stable after the composite formation process [31,32].

The absorption band at 1380,81 cm^{-1} is attributed to C–H bending vibrations of aliphatic groups or residual organic compounds remaining on the biochar surface [34]. Meanwhile, the band at 1044,48 cm^{-1} corresponds to C–O stretching vibrations of alcohol, phenolic, or ester groups, confirming the presence of active oxygen-containing functional groups on the biochar surface [35]. These oxygen functional groups play a crucial role in the adsorption of Fe metal ions through electrostatic interactions and surface complexation mechanisms [33,35].

The main characteristics of the $MnFe_2O_4$ composite are evidenced by absorption bands in the low-frequency region at 572,20 cm^{-1} and 500 cm^{-1}, which correspond to metal–oxygen (M–O) vibrations and are typically assigned to Mn–O and Fe–O stretching modes in the spinel $MnFe_2O_4$ structure [36,37]. The appearance of these bands confirms the successful formation of the $MnFe_2O_4$ spinel phase and indicates that its presence is not obscured by organic compounds originating from the biochar [3].

Antibacterial Activity

Antibacterial activity tests were conducted to evaluate the ability of the biochar/$MnFe_2O_4$ composite to inhibit the growth of *Escherichia coli* (Gram-negative) and *Staphylococcus aureus* (Gram-positive), which are commonly used indicator microorganisms in antibacterial material effectiveness studies [38,39]. The results of antibacterial activity tests are presented in **Figure 6**, while the inhibition zone diameters for each treatment are summarized in **Table 2.**

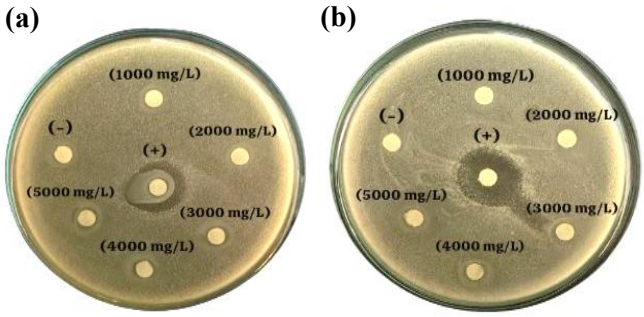

Figure 6. Biochar/$MnFe_2O_4$ nanocomposite for antibacterial activity of (a) *E.coli*, (b) *S.aureus*.

Table 2. Biochar/$MnFe_2O_4$ nanocomposite for antibacterial activity of (a) *E.coli*, (b) *S.aureus*

Nanocomposite Concentration (mg/L)	*E. Coli* (mm)	*S. Aureus* (mm)
Amoxicillin Positive Control (1000 mg/L)	18.5±0.5	18.0±0.0
DMSO Negative Control (1000 mg/L)	6.0±0.0	6.0±0.0
Nanocomposite 1000 mg/L	6.0±0.0	6.0±0.0
Nanocomposite 2000 mg/L	6.2±0.1	6.2±0.1
Nanocomposite 3000 mg/L	6.7±0.2	6.5±0.2
Nanocomposite 4000 mg/L	6.8±0.1	6.8±0.1
Nanocomposite 5000 mg/L	7.2±0.3	7.2±0.3

Antibacterial activity of the biochar/$MnFe_2O_4$ composite against *Escherichia coli* and *Staphylococcus aureus* is presented in **Figure 6** and summarized in **Table 2** (mean ± standard deviation, n = 3). The positive control (amoxicillin, 1000 mg/L) produced pronounced inhibition zones of 18.5 ± 0.5 mm for *E. coli* and 18.0 ± 0.0 mm for *S. aureus*, confirming the validity of the disc diffusion method. In contrast, the negative control (DMSO) exhibited a 6.0 ± 0.0 mm inhibition zone, corresponding to the diameter of the paper disc, indicating the absence of

intrinsic antibacterial activity from the solvent [40], [41].

For the biochar/$MnFe_2O_4$ composite, the inhibition zone increased gradually with increasing concentration. However, even at the highest concentration (5000 mg/L), concentrations are expressed in mg/L based on suspension concentration prior to disc loading, the inhibition zone reached only 7.2 ± 0.3 mm, corresponding to approximately 1.2 mm beyond the disc diameter. This result clearly indicates that the antibacterial potency of the composite remains relatively weak compared to conventional antibiotics. Therefore, the antibacterial performance can be categorized as weak based on disc diffusion criteria [42].

The modest antibacterial activity observed is consistent with previous reports indicating that biochar-based materials generally exhibit limited intrinsic bactericidal properties and primarily function as adsorptive or surface-active matrices rather than strong antimicrobial agents [1,39]. The porous structure of rice husk-derived biochar enhances bacterial adsorption and increases the contact interface between microbial cells and active particles. Surface functional groups such as –OH and C=O facilitate electrostatic interactions and may contribute to membrane destabilization [43,44].

The incorporation of $MnFe_2O_4$ introduces redox-active sites capable of generating reactive oxygen species (ROS) through Mn^{2+}/Fe^{3+} cycling within the spinel structure. Previous studies have demonstrated that manganese ferrite nanoparticles can induce oxidative stress, membrane disruption, and intracellular damage via ROS production [6,7,45]. Nevertheless, antibacterial efficiency strongly depends on nanoparticle dispersion, surface accessibility, and ferrite loading.

XRD analysis confirmed the formation of nanocrystalline $MnFe_2O_4$ with an average crystallite size of approximately 27.1 nm, which is favorable for surface-mediated catalytic reactions [7,25]. However, SEM observations revealed partial particle agglomeration within the biochar matrix, potentially reducing the effective exposure of active ferrite domains. EDX analysis verified the presence and homogeneous distribution of Mn and Fe elements, yet the accessible catalytic sites may still be insufficient to produce strong bactericidal effects. These structural factors likely contribute to the relatively small inhibition zones observed in this study. The antibacterial mechanism is therefore proposed to be synergistic rather than purely bactericidal, as illustrated in **Figure 7.**

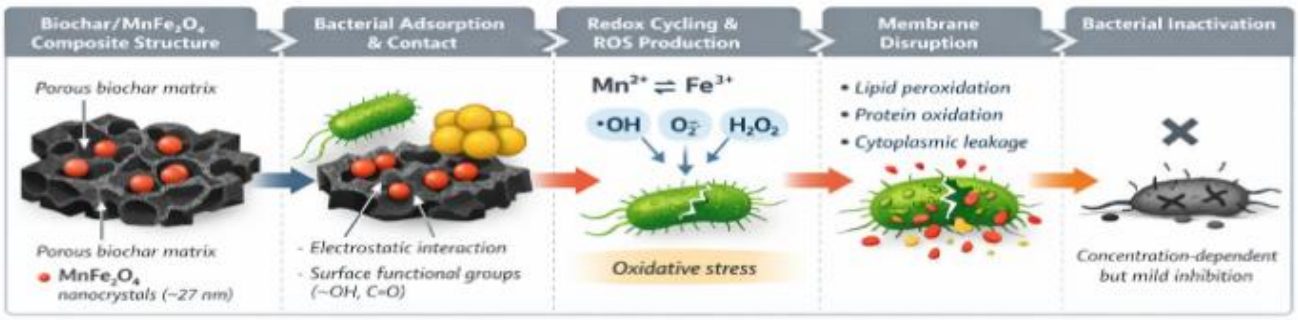

Figure 7. Antibacterial Mechanism of Biochar/$MnFe_2O_4$ Composite

The antibacterial mechanism is therefore proposed to be synergistic rather than purely bactericidal, as illustrated in **Figure 7**. The porous biochar framework enhances bacterial adsorption and promotes close contact between cells and $MnFe_2O_4$ nanoparticles, while the ferrite phase generates localized oxidative stress via ROS formation. Similar synergistic concepts have been reported in magnetic biochar systems designed for environmental remediation applications [13,14,46]. This contact–oxidative mechanism explains the concentration-dependent but limited antibacterial response observed in the disc diffusion.

Overall, although the antibacterial activity of the rice husk-derived biochar/$MnFe_2O_4$ composite remains modest compared to standard antibiotics, the material demonstrates measurable and concentration-dependent inhibition. Its main advantages include eco-friendly composition, magnetic separability, and the utilization of abundant agricultural biomass waste [1,46,47]. With further optimization of ferrite loading, nanoparticle dispersion, and surface functionalization, the composite holds as a multifunctional material for sustainable environmental protection applications.

CONCLUSION

The rice husk-derived biochar/$MnFe_2O_4$ composite was successfully synthesized via the coprecipitation method, demonstrating the effective integration of magnetic $MnFe_2O_4$ onto the biochar matrix. Structural characterization confirmed the formation of a stable cubic spinel $MnFe_2O_4$ phase, while SEM analysis revealed uniform nanoparticle dispersion on the porous biochar surface. FTIR results further verified the presence of surface functional groups (–OH, C=O, and C–O) and characteristic Mn–O and Fe–O vibrations, confirming successful composite formation and interfacial interactions. Antibacterial evaluation against *Escherichia coli* (Gram-negative) and *Staphylococcus aureus* (Gram-positive) showed a dose-dependent but modest antibacterial activity, with a maximum inhibition zone of 7.2 mm at 5000 mg/L. The observed activity is attributed to the synergistic effects of reactive oxygen species (ROS) generation by $MnFe_2O_4$ and the porous biochar structure that enhances bacterial contact. Importantly, the composite combines antibacterial functionality with magnetic separability, enabling easy recovery and reuse, while utilizing rice husk agricultural waste as a sustainable precursor. These features highlight its potential contribution to environmentally friendly material development and waste valorization strategies. Future studies will focus on improving antibacterial performance through structural optimization, such as particle size reduction, elemental doping, and enhanced nanoparticle dispersion, while further exploring its applicability in sustainable environmental applications.

ACKNOWLEDGMENT

The authors acknowledgment the financial support from Universitas Sriwijaya under the 2025 Competitive Research Scheme (Contract No. 0028/UN9/LPPM.PT/2025, September 17, 2025 and the BRIN Tangerang Laboratory for granting permission and providing full support for the completion of this research.

REFERENCES

[1] D. Mukherjee, M. Sil, A. Goswani, D. Bhattacharya, M. Nag, D. Lahiri, K. Sharma, and R. Verma, "Synthesis, modification and antimicrobial potential of biochar and its modifications against water-borne pathogens: A review," *Results in Surfaces and Interfaces*, vol. 18, pp. 100438, 2025.

[2] M. Liu, L. Guan, Y. Wen, L. Su, Z. Hu, Z. Peng, S. Li, Q. Tang, Z. Zhou, and N. Zhou, "Rice husk biochar mediated red phosphorus for photocatalysis and photothermal removal of E. coli," *Food Chemistry*, vol. 410, pp. 135455, 2023.

[3] S.Y. Lee, H. Kim, H. Jang, M.J. Hwang, K.B. Lee, J.W. Choi, and K.W. Jung, "Fabrication of manganese ferrite ($MnFe_2O_4$) microsphere-coated magnetic biochar composite for antimonate sequestration: Characterization, adsorption behavior, and mechanistic understanding," *Applied Surface Science*, vol. 578, pp. 152005, 2022.

[4] G. Subbiah, R. Pratap Singh, K. Deepak, P.P. Nayak, K. Venkadeshwaran, A. Tiwari, J. Sahoo, and K. Priya K, "Continuous pyrolysis of rice husk for sustainable biochar production and carbon sequestration: Recent advances and techno-economic perspectives," *Results in Engineering*, vol. 27, pp. 106991, 2025.

[5] J. Sun, W. Yan, X. Liu, T. Hu, Y. Xiong, S. Tian, J. Feng, Z. Huang, and Z. Zhao, "Rice husk waste-derived super-biochar with the max surface area and Philic-CO_2 textural structure: Boosting effect and mechanism of post-desilication," *Chemical Engineering Journal*, vol. 490, pp. 151583, 2024.

[6] E.H.M. Sakho, J. Jose, S. Thomas, N. Kalarikkal, and O.S. Oluwafemi, "Antimicrobial properties of MFe_2O_4 (M = Mn, Mg)/reduced graphene oxide composites synthesized via solvothermal method," *Materials Science and Engineering C*, vol. 95, pp. 43–48, 2019.

[7] S.D. Bharathi and D.R. Babu, "Synthesis, characterization and antimicrobial activity of Manganese ferrite nanoparticles," *Materials Science and Engineering B*, vol. 300, pp. 117051, 2024.

[8] S.J. Salih and Z.S. Tahseen, "Next Sustainability Spinel ferrite nanoparticles in environmental remediation : Adsorption, catalysis, and sustainability perspectives," *Next Sustainability*, vol. 7, pp. 100240, 2026.

[9] C. Lai Cui, F. Huang, G. Zeng, D. Huang, L. Qin, M. Cheng, C. Zhang, B. Li, H. Yi, S. Liu, L. Li, and L. Chen, "Fabrication of novel magnetic $MnFe_2O_4$/bio-char composite and heterogeneous photo-Fenton degradation of tetracycline in near neutral pH," *Chemosphere*, vol. 224, pp. 910–921, 2019.

[10] Z. Wen, J. Xi, J. Lu, Y. Zhang, G. Cheng, Y. Zhang, and R. Chen, "Porous biochar-supported $MnFe_2O_4$ magnetic nanocomposite

as an excellent adsorbent for simultaneous and effective removal of organic/inorganic arsenic from water," *Journal of Hazardous Materials*, vol. 411, pp. 124909, 2021.

[11] G. Fuat and Y. Cumali, "Synthesis, characterization, and lead (II) sorption performance of a new magnetic separable composite: $MnFe_2O_4$@wild plants-derived biochar," *Journal of Environmental Chemical Engineering*, vol. 9, pp. 104567, 2021.

[12] A. Choudhry, A. Sharma, S.I. Siddiqui, I. Ahamad, Md. Sajid, T.A. Khan, and S.A. Chaudhry, "Origanum vulgare manganese ferrite nanocomposite: An advanced multifunctional hybrid material for dye remediation," *Environmental Research*, vol. 220, pp. 115193, 2023.

[13] X. Li, C. Wang, J. Zhang, J. Liu, B. Liu, and G. Chen, "Preparation and application of magnetic biochar in water treatment: A critical review," *Science of the Total Environment*, vol. 711, pp. 134847, 2020.

[14] Y. Yi, Z. Huang, B. Lu, J. Xian, E. P. Tsang, W. Cheng, J. Fang, Z. Fang, "Magnetic biochar for environmental remediation: A review," *Bioresource Technology*, vol. 298, pp. 122468, 2020.

[15] Z. Wang, Y. Li, X. Xie, and Z. Wang, "Bifunctional $MnFe_2O_4$/chitosan modified biochar composite for enhanced methyl orange removal based on adsorption and photo-Fenton process," *Colloids and Surfaces A: Physicochemical and Engineering Aspects*, vol. 613, pp. 126104, 2021.

[16] H. Hinsene, N. Bhawawet, and A. Imyim, "Rice husk biochar doped with deep eutectic solvent and Fe_3O_4/ZnO nanoparticles for heavy metal and diclofenac removal from water," *Separation and Purification Technology*, vol. 339, pp. 126638, 2024.

[17] Y. Wang, H. Jiao, Z. Liu, S. Yang, R. Chen, C. Liu, J. Dai, and D. Din, "Biochar alters the selectivity of $MnFe_2O_4$-activated periodate process through serving as the electron-transfer mediator," *Journal of Hazardous Materials*, vol. 472, pp. 134530, 2024.

[18] D.N. Tharaka, N.D. Tissera, G. Priyadarshana, and D. Dahanayake, "A Comprehensive Review of Hierarchical Porous Carbon Synthesis from Rice Husk," *Rice Science*, vol. 32, pp. 499–511, 2025.

[19] S.V. Singh, S. Chaturvedi, V.C. Dhyani, and G. Kasivelu, "Pyrolysis temperature influences the characteristics of rice straw and husk biochar and sorption/desorption behaviour of their biourea composite," *Bioresource Technology*, vol. 314, pp. 123674, 2020.

[20] C. Jin, X. Chen, S. Sun, Y. Liu, and B. Hu, "Simultaneous removal of Cd(II) and Sb(V) by $MnFe_2O_4$-biochar composite: Performance and mechanisms," *Ecotoxicology and Environmental Safety*, vol. 294, pp. 118093, 2025.

[21] O. Hakami, "Structural, dielectric and magnetic properties of $MnFe_2O_4$/ MWCNTs based nanocomposites for technological applications," *Surfaces and Interfaces*, vol. 49, pp. 104387, 2024.

[22] L. Gao, Z. Liu, Z. Yang, L. Cao, C. Feng, M. Chu, and J. Tang, "Synthesis and magnetism property of manganese ferrite $MnFe_2O_4$ by selective reduction and oxidization roasting process," *Applied Surface Science*, vol. 508, pp. 145292, 2020.

[23] N. Akechatree, K. Lakshmanan, R. Rajendran, T. Rojviroon, O. Rojviroon, and S. Sirivithayapakorn, "Bifunctional $MnFe_2O_4$/g-C_3N_4 nanocomposites for synergistic electrocatalytic oxygen evolution and photocatalytic organic dye degradation," *Journal of Water Process Engineering*, vol. 77, pp. 108590, 2025.

[24] T.J. Antony, K. Thirunavukkarasu, and K. Jagannathan, "Structural, morphological and magnetic analysis of hydrothermally synthesized $MnFe_2O_4$ magnetic nanoferrites," *Materials Today: Proceedings*, vol. 10, pp. 2–5, 2023.

[25] P.A. Vinosha, B. Xavier, D. Anceila, and S.J. Das, "Optik Nanocrystalline ferrite (MFe_2O_4, M=Ni, Cu, Mn and Sr) photocatalysts synthesized by homogeneous Co-precipitation technique," *Optik - International Journal for Light and Electron Optics*, vol. 157, pp. 441-448, 2018.

[26] F. Hamidi and L. E. Tunstall, "Insights into the influence of biochar powder on the fresh state properties and strength development of concrete," *Construction and Building Materials*, vol. 498, pp. 144006, 2025.

[27] S. Rajendran, G. Palani, A. Veerasimman, V. Shanmugam, U. Marimuthu, K. Korniejenko, H. Trilaksana, A. Majumder, and F. Stochino, "Enhancing carbon fiber composites with fish scale biochar for superior strength and environmental sustainability," *Cleaner*

Engineering and Technology, vol. 27, pp. 100996, 2025.

[28] H.H.P. Quang, P.K.T. Nguyen, P. Singh, P. Raizada, and V.H. Nguyen, "Engineered boron-doped biochar for sustainable environmental remediation and circular energy systems: A review," *Journal of Environmental Chemical Engineering*, vol. 13, pp. 118194, 2025.

[29] H. Dhila, A. Bhapkar, and S. Bhame, "Metal oxide/biochar hybrid nanocomposites for adsorption and photocatalytic degradation of textile dye effluents: A review," *Desalination and Water Treatment*, vol. 321, pp. 101004, 2025.

[30] T.U. Vandana, B.K. Tripathy, R.K. Mishra, A. Sharma, and K. Mohanty, "A review on waste biomass-derived biochar: Production, characterisation, and advanced analytical techniques for pollutants assessment in water and wastewater," *Process Safety and Environmental Protection*, vol. 201, pp. 107505, 2025.

[31] O.M. Rodriguez-Narvaez, J.M. Peralta-Hernandez, A. Goonetilleke, and E.R. Bandala, "Biochar-supported nanomaterials for environmental applications," *Journal of Industrial and Engineering Chemistry*, vol. 78, pp. 21–33, 2019.

[32] R. Janu, V. Mrlik, D. Ribitsch, J. Hofman, P. Sedlacek, L. Bielska, G. Soja, "Biochar surface functional groups as affected by biomass feedstock, biochar composition and pyrolysis temperature," *Carbon Resources Conversion*, vol. 4, pp. 36–46, 2021.

[33] P. Tu, G. Zhang, G. Wei, J. Li, Y. Li, L. Deng, and H. Yuan, "Influence of pyrolysis temperature on the physicochemical properties of biochars obtained from herbaceous and woody plants," *Bioresources and Bioprocessing*, vol. 9, pp. 131, 2022.

[34] M. Masuku, J.F. Nure, H.I. Atagana, N. Hlongwa, and T.T.I. Nkambule, "Pinecone biochar for the Adsorption of chromium (VI) from wastewater: Kinetics, thermodynamics, and adsorbent regeneration," *Environmental Research*, vol. 258, pp. 119423, 2024.

[35] M. Shafiq, A.A. Alazba, and M.T. Amin, "Eco-friendly nanocomposite of manganese-iron and plant waste derived biochar for optimizing Pb^{2+} adsorption: A response surface methodology approach," *Desalination and Water Treatment*, vol. 322, pp. 101091, 2025.

[36] P. Gole, K. Raut, and B. Kandasubramanian, "Polymer-based biochar materials for environmental remediation: A review," *Hybrid Advances*, vol. 6, pp. 100267, 2024.

[37] M.R Rajani, R. Ravishankar, K.M. Naik, S. Raghavan M, C. Vidya, G. Kumar S, and C. Manjunatha, "Carbonaceous $MnFe_2O_4$ nano-adsorbent: Synthesis, characterisation and investigations on chromium (VI) ions removal efficiency from aqueous solution," *Applied Surface Science Advances*, vol. 16, pp. 100434, 2023.

[38] M. Faizan, M.Y. Naz, S.A.S.A. Shah, I. Shakir, M. Khaliq, M.A. Busharat, and D. Pan, "Mesoporous magnetic $MnFe_2O_4$@SiO_2-chitosan nanocomposite for efficient adsorptive removal of Zn(II) and Cd(II) ions from aqueous media," *Desalination and Water Treatment*, vol. 324, pp. 101488, 2025.

[39] R. Das and S.N. Panda, "Preparation and applications of biochar based nanocomposite: A review," *Journal of Analytical and Applied Pyrolysis*, vol. 167, pp. 105691, 2022.

[40] J. Wang, R. Qiang, Q. Miao, R. Hu, H. Chen, S. Guo, and Z. Liu, "Synthesis and potent antibacterial activity of nano-$CuFe_2O_4$/MoS_2@Ag composite under visible light," *Applied Surface Science*, vol. 684, pp. 161908, 2025.

[41] M. Bhat, B. Chakraborty, R.S. Kumar, A.I. Almansour, N. Arumugam, D. Kotresha, S.S. Pallavi, S.B. Dhanyakumara, K.N. Shashiraj, and S. Nayaka, "Biogenic synthesis, characterization and antimicrobial activity of Ixora brachypoda (DC) leaf extract mediated silver nanoparticles," *Journal of King Saud University - Science*, vol. 33, pp. 101296, 2021.

[42] S. Vihodceva, A. Sutka, M. Iesalnieks, M. Sihtmae, A. Nefedova, A. Ivask, I. Blinova, M. Maiorov, M. Vanags, T.V. Eiduks, A. Pludons, A. Kahru, and K. Kasemets, "Synthesis and antimicrobial efficacy of magnetic $CuO/Fe_2O_3/CuFe_2O_4$ nanostructured composite: Mechanisms of action, cytotoxicity to human keratinocytes in vitro, and ecotoxicity towards Vibrio fischeri and Daphnia magna," *Journal of Environmental Chemical Engineering*, vol. 13, pp. 117991, 2025.

[43] X. Dong, Y. Chu, Z. Tong, M. Sun, D. Meng, X. Yi, T. Gao, M. Wang, and J. Duan, "Mechanisms of adsorption and

functionalization of biochar for pesticides: A review," *Ecotoxicology and Environmental Safety*, vol. 272, pp. 116019, 2024.

[44] E. Hashemi, M.M. Norouzi, and M. Sadeghi-Kiakhani, "Magnetic biochar as a revolutionizing approach for diverse dye pollutants elimination: A comprehensive review," *Environmental Research*, vol. 261, pp. 119548, 2024.

[45] P. Ning, C.C. Liu, Y.J. Wang, X.Z. Li, R. Ranjithkumar, Z.H. Gan, Y.Y. Wu, and T. Fu, "Facile synthesis, antibacterial mechanisms and cytocompatibility of Ag-$MnFe_2O_4$ magnetic nanoparticles," *Ceramics International*, vol. 46, pp. 20105–20115, 2020.

[46] K. Kang, Y. Hu, I. Khan, S. He, and P. Fatehi, "Recent advances in the synthesis and application of magnetic biochar for wastewater treatment," *Bioresource Technology*, vol. 390, pp. 129786, 2023.

[47] Y. Trivedi, M. Sharma, R.K. Mishra, A. Sharma, J. Joshi, A.B. Gupta, B. Achintya, K. Shah, and A.K. Vuppaladadiyamd, "Biochar potential for pollutant removal during wastewater treatment: A comprehensive review of separation mechanisms, technological integration, and process analysis," *Desalination*, vol. 600, pp. 118509, 2025.